VOLUME 117, NUMBER 22
JUNE 7, 1995

JOURNAL OF THE AMERICAN CHEMICAL SOCIETY

Solution Structure of the Menogaril–DNA Complex

Huifen Chen[†] and Dinshaw J. Patel*[,†,‡]

Contribution from the Department of Biochemistry and Molecular Biophysics, College of Physicians and Surgeons of Columbia University, New York, New York 10032, and Cellular Biochemistry and Biophysics Program, Memorial Sloan-Kettering Cancer Center, New York, New York 10021

Received February 13, 1995[⊗]

Abstract: Menogaril (7-*con*-*O*-methylnogarol) is a derivative of the anthracycline antitumor drug nogalamycin lacking both the nogalose sugar and acetyl functionality that are positioned in the minor groove of the nogalamycin–DNA complex. Two menogaril molecules bind to the self-complementary d(G1-A2-C3-A4-T5-G6-T7-C8) duplex in a cooperative manner and form a symmetric two drugs per duplex complex. We have obtained the solution structure of the menogaril–d(G-A-C-A-T-G-T-C) complex by a combined NMR–molecular dynamics study including intensity-based refinement. The aglycon chromophore of menogaril intercalates between (C3-A4)·(T5-G6) base pairs, with its long axis orthogonal to the long axis of the flanking Watson–Crick base pairs. The B, C, and D aromatic rings of the aglycon chromophore stack primarily with the G6 base with the OH-4/OH-6 bearing edge directed toward the C3-A4 strand, while the nonplanar cyclohexene ring A protrudes into the minor groove and adopts a half-chair conformation. An intermolecular hydrogen bond is detected between the OH-9 of the cyclohexene ring A and O2P of the G6-T7 step in the minor groove. The positively charged bicyclic aminoglucose sugar which is fused to the aromatic ring D of the aglycon is positioned in the major groove and spans the three base pair d(A2-C3-A4)·d(T5-G6-T7) segment. The aminoglucose sugar adopts a chair conformation with the bridgehead oxygen atom directed toward the A4·T5 base pair and the charged $N(CH_3)_2$-3″ group directed toward the A2·T7 base pair. A strong intermolecular hydrogen bond is detected between the OH-2″ of the bicyclic aminoglucose sugar and the N7 of G6 in the major groove, which accounts for the sequence specificity of menogaril for its target sites on DNA. Intercalation of the aglycon of menogaril through the major groove contrasts with the majority of antitumor antibiotics which intercalate into DNA through the minor groove.

Introduction

The anthracycline family of antitumor antibiotics have been used clinically as components in combination chemotherapeutic treatments for a wide variety of cancers.[1] The anthracyclines consist of an aglycon chromophore capable of intercalating into DNA and a charged amino sugar covalently linked to the nonplanar cyclohexene ring at one end of the aglycon. A prominent member of this family is doxorubicin whose chemical structure is shown in **1**. Minor chemical modifications in the charged amino sugar have pronounced effects on the clinical efficacy within the anthracycline family of antitumor antibiotics.[1]

Nogalamycin (**2**), isolated from *Streptomyces nogalator*,[2] is larger and more complex than the simpler anthracycline **1** since it contains substituents at both ends of the aglycon chromophore. An uncharged nogalose sugar is attached to the cyclohexene

[†] Columbia University.
[‡] Memorial Sloan-Kettering Cancer Center.
* Address correspondence to this author at the Memorial Sloan-Kettering Cancer Center.
[⊗] Abstract published in *Advance ACS Abstracts*, May 15, 1995.
(1) Acramone, F.; Penco, S. In *Anthracyclines and Anthracenedione-based Anticancer Agents*; Lown, J. W., Ed.; Elsevier: New York, 1988; pp 1–43.
(2) Bhuyan, B. K.; Deitz, A. *Antimicrob. Agents Chemother.* **1965**, 836–844.

0002-7863/95/1517-5901$09.00/0

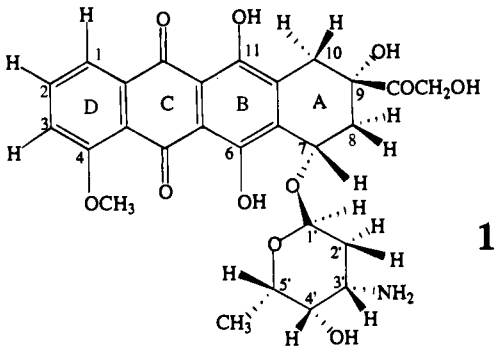

1

doxorubicin

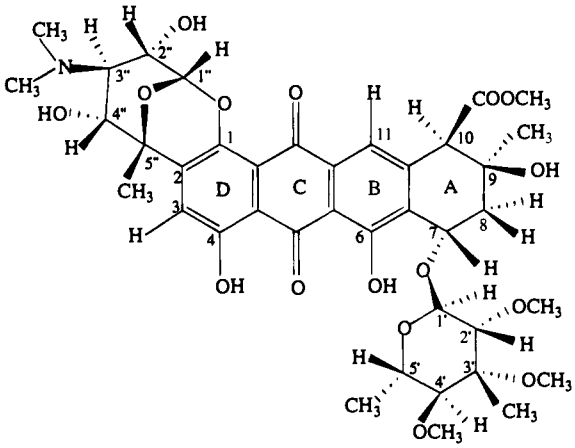

2

nogalamycin

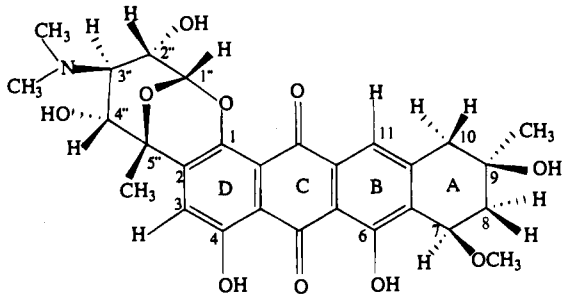

3

menogaril

ring A at one end of the aglycon while a positively charged bicyclic aminoglucose sugar is fused to aromatic ring D at the other end of the aglycon[3] in **2**. Support for DNA as a target site for the antitumor activity of nogalamycin is based on its selective inhibition of DNA-directed RNA synthesis *in vivo*.[4]

Nogalamycin forms stable intercalative complexes with duplex DNA[5] and exhibits slow association and dissociation rates[6] consistent with barriers to the insertion and release of the dumbbell-shaped molecule into DNA. Footprinting studies have established that nogalamycin binds preferentially to alternating pyrimidine–purine sites on DNA[7] with sequence specificity for (C-A)·(T-G) steps demonstrated from *in vitro* transcription assay measurements.[8]

Early NMR studies established that nogalamycin binds to duplex DNA through intercalation of its aglycon at either (C-A)·(T-G)[9] or (C-G)·(C-G)[10,11] steps with positioning of the nogalose sugar in the minor groove and the bicyclic aminoglucose sugar in the major groove. High-resolution views of nogalamycin–DNA oligomer complexes have emerged from X-ray studies in the crystalline[12,13] and NMR studies[14,15] in the solution state. These studies established that the aglycon intercalates between pyr (3′–5′) pur steps with its long axis orthogonal to the long axis of the flanking base pairs. The nogalose sugar, the cyclohexene ring A, and the acetyl functionality form a continuous domain which aligns through van der Waals interactions with the walls of the minor groove. The charged bicyclic aminoglucose sugar is positioned in the major groove with its hydroxyl functionalities directed toward and hydrogen bonding with the base pair edges of flanking G·C pairs.

Nogalamycin is active against a variety of rodent tumors and leukemias.[2,16] However, it displays unacceptable levels of renal and pulmonary toxicity and venous occlusion in mammals.[17] A large number of nogalamycin analogs have been screened of which only 7(*R*)-*O*-methylnogarol or menogaril (**3**) has been found to be highly active against a wide spectrum of experimental tumors and leukemias *in vivo*.[18] Further, this antitumor activity was manifested at every phase in the cell cycle and was independent of the route of administration. Menogaril was also found to be active against a multi-drug resistant human breast tumor cell line under conditions where resistance was observed for the anthracycline doxorubicin.[19] Menogaril is currently being tested in several phase II clinical trials on patients with metastatic breast cancer.

Menogaril (**3**) lacks both the acetyl functionality and the nogalose sugar which are attached covalently to the cyclohexene ring A in nogalamycin (**2**) and, in addition, has reversed stereochemistry at the C7 position on the aglycon ring. These are the nogalamycin functionalities that were identified with van der Waals interactions in the minor groove of the nogalamycin–DNA complex. Menogaril (**3**) retains the charged bicyclic aminoglucose sugar of nogalamycin (**2**) which interacts with the major groove through intermolecular hydrogen bonding interactions and presumably accounts for the sequence specific-

(3) Arora, S. K. *J. Am. Chem. Soc.* **1983**, *105*, 1328–1332.
(4) (a) Fok, J.; Waring, M. J. *Mol. Pharmacol.* **1972**, *8*, 65–74. (b) Li, L. H.; Kuentzel, S. L.; Murch, L. L.; Pschigoda, L. M.; Krueger, W. C. *Cancer Res.* **1979**, *39*, 4816–4822. (c) Ennis, H. L. *Antimicrob. Agents Chemother.* **1981**, *19*, 657–665.
(5) (a) Kersten, W.; Kersten, H.; Szybalski, W. *Biochemistry* **1966**, *5*, 236–244. (b) Waring, M. J. *J. Mol. Biol.* **1970**, *54*, 247–279. (c) Plumbridge, R. W.; Brown, J. R. *Biochem. Pharmacol.* **1979**, *28*, 3231–3234.
(6) (a) Fox, K. R.; Waring, M. J. *Biochim. Biophys. Acta* **1984**, *802*, 162–168. (b) Fox, K. R.; Brassett, C.; Waring, M. J. *Biochim. Biophys. Acta* **1985**, *840*, 383–392.
(7) (a) Fox, K. R.; Waring, M. J. *Biochemistry* **1986**, *25*, 4349–4356. (b) Fox, K. R.; Alam, Z. *Eur. J. Biochem.* **1992**, *209*, 31–36.
(8) White, R. J.; Phillips, D. R. *Biochemistry* **1989**, *28*, 4277–4293.
(9) Searle, M. S.; Hall, J. G.; Denny, W. A.; Wakelin, L. P. G. *Biochemistry* **1988**, *27*, 4340–4349.
(10) Robinson, H.; Liaw, Y.-C.; van der Marel, G. A.; van Boom, J. H.; Wang, A. H.-J. *Nucleic Acids Res.* **1990**, *18*, 4851–4858.
(11) van Houte, L. P. A.; van Garderen, C. J.; Patel, D. J. *Biochemistry* **1993**, *32*, 1667–1674.
(12) (a) Gao, Y.-G.; Liaw, Y.-C.; Robinson, H.; Wang, A. H.-J. *Biochemistry* **1990**, *29*, 10307–10316. (b) Liaw, Y.-C.; Gao, Y.-G.; Robinson, H.; van der Marel, G. A.; van Boom, J. H.; Wang, A. H.-J. *Biochemistry* **1989**, *28*, 9913–9918.
(13) (a) Williams, L. D.; Egli, M.; Gao, Q.; Bash, P.; van der Marel, G. A.; van Boom, J. H.; Rich, A.; Frederick, C. A. *Proc. Natl. Acad. Sci. U.S.A.* **1990**, *87*, 2225–2229. (b) Egli, M.; Williams, L. D.; Frederick, C. A.; Rich, A. *Biochemistry* **1991**, *30*, 1364–1372.
(14) Zhang, X.; Patel, D. J. *Biochemistry* **1990**, *29*, 9451–9466.
(15) Searle, M. S.; Bicknell, W. *Eur. J. Biochem.* **1992**, *205*, 45–58.
(16) (a) Bhuyan, B. K. In *Antibiotics*; Gottlieb, D., Shaw, P. D., Eds.; Springer: New York, 1967; Vol. 1, pp 173–180. (b) Bhuyan, B. K.; Reusser, F. *Cancer Res.* **1970**, *30*, 984–989. (c) Brown, J. R. In *Molecular Aspects of Anti-Cancer Drug Action*; Neidle, S., Waring, M. J., Eds.; Macmillan: London, 1983; pp 57–92.
(17) Bhuyan, B. K.; Smith, C. G. In *Antineoplastic and Immunosuppressive Agents*; Sartorelli, A. C., Johns, D. G., Eds.; Springer-Verlag: Berlin, 1975; Part II, pp 623–632.
(18) Bhuyan, B. K.; McGovren, J. P.; Crampton, S. L. *Cancer Res.* **1981**, *41*, 882–887.
(19) Sinha, B. K.; Atwell, J.; Politi, P. M. *Chem.-Biol. Interact.* **1990**, *76*, 89–99.

ity of complex formation. In essence, menogaril (**3**) contains an intercalating aglycon chromophore with an attached major groove binding charged bicyclic aminoglucose sugar, in contrast to the anthracycline doxorubicin (**1**), which contains an intercalating aglycon chromophore with an attached minor groove binding charged amino sugar. Structural studies of the menogaril–DNA complex are of great interest since there are no examples of natural drugs intercalating solely from the major groove despite the fact that the majority of proteins bind to the major groove of DNA.

We report below on a high-resolution structural study of the menogaril–d(G-A-C-A-T-G-T-C) complex (two drugs bound per duplex) using a combined NMR–molecular dynamics approach including intensity-based refinement.

Experimental Section

Oligonucleotide Synthesis. The self-complementary deoxyoligonucleotide **4** was synthesized on an Applied Biosystems Model 391 DNA synthesizer using the solid phase β-cyanoethyl phosphoramidite chemistry at the 10 μmol scale. The crude 5′-dimethoxytritylated

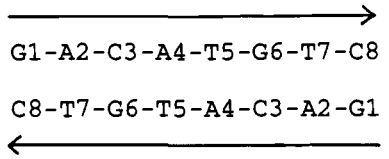

4

(DMT) oligonucleotide was obtained by treating the solid support in concentrated ammonia for 16 h at 55 °C and then purified by reverse-phase HPLC in two stages with the DMT protecting group initially on and subsequently removed. The purified product was converted into the Na^+ form by passing through a Sephadex G-25 column and a Dowex cation-exchange resin column.

Formation of the Menogaril–DNA Complex. The menogaril sample was provided by the Upjohn Co., Kalamazoo, MI. Menogaril was gradually added to the self-complementary d(G-A-C-A-T-G-T-C) duplex, and complex formation was monitored by recording the one-dimensional proton NMR spectrum in H_2O buffer. The titration was complete on addition of two menogarils per duplex. The buffer was 0.1 M NaCl, 10 mM phosphate, and 1 mM EDTA.

NMR Experiments. All one- and two-dimensional NMR experiments on the menogaril–DNA complex were recorded on a Bruker AMX 500 spectrometer. The two-dimensional spectra were processed using the FELIX (Biosym Technologies, Inc.) software packages on an IRIS-INDIGO workstation (Silicon Graphics, Inc.). All proton chemical shifts were referenced relative to internal sodium 2,2-dimethyl-2-silapentane-5-sulfonate (DSS), and phosphorus chemical shifts were referenced relative to external trimethyl phosphate (TMP) reference standards.

Two-dimensional phase-sensitive NOESY experiments on the complex in H_2O buffer were acquired at 80 and 150 ms mixing times at 10 °C. The data were collected with a sweep width of 20 ppm in each dimension with the carrier frequency placed on the H_2O resonance. In both experiments, 70° excitation and mixing pulses were used and suppression of the H_2O signal was obtained by a jump-and-return pulse sequence.[20] The waiting time between the two pulses in the jump-and-return sequence was about 56 μs to obtain maximum excitation centered about the imino proton resonances. A 30 ms homospoil pulse was used in the middle of the mixing period to further suppress the H_2O resonance. A total of 1024 complex data points were collected in the t_2 dimension and 256 complex data points were collected in the t_1 dimension in the hypercomplex mode.[21] A skewed sine-bell window function was used in processing the data.

NOESY experiments on the complex in D_2O buffer were acquired at 25 °C with a mixing time of 250 ms and at 10 °C with mixing times of 30, 60, 100, 150, and 200 ms. The latter five NOESY experiments were NOE buildup data sets recorded consecutively under the same experimental conditions. These were used in deriving proton–proton distances and NOE intensity restraints. The data were acquired with 1024 complex data points in t_2 and 512 real data points in t_1 in the phase-sensitive TPPI mode.[22] The carrier was placed on the residual HDO signal, and solvent suppression was achieved by low-power continuous-wave irradiation during the relaxation delay. The buildup experiments were processed with a 90° phase-shifted sine-bell window function in both t_2 and t_1 dimensions and baseline correction in the t_2 dimension.

Correlated (DQF-COSY and COSY-45) spectra were acquired in the phase-sensitive TPPI mode[22] on the complex in D_2O buffer at 25 °C. In the COSY-45 experiment, a 8 ppm sweep width was used and 2048 complex data points in the t_2 dimension and 600 increments in the t_1 dimension were collected. A 0° phase-shifted sine-bell window function was multiplied to the free induction decay before Fourier transformation. Homonuclear TOCSY[23] and "Clean"-TOCSY[24] experiments were recorded at 50 and 100 ms mixing times, respectively.

A proton-detected $^1H-^{31}P$ heteronuclear correlation experiment[25] on the complex in D_2O buffer was recorded at 25 °C. The spectral width in the t_2 proton dimension was 9 ppm, and 1024 complex data points were collected. The spectral width in the t_1 phosphorus dimension was 6 ppm, and 320 increments were collected in the TPPI mode.[22]

Interproton Distance and Intensity Restraints. The distance restraints involving nonexchangeable protons were obtained from buildup rates of the nuclear Overhauser effect (NOE) cross peaks observed in NOESY spectra of the complex in D_2O buffer at 10 °C acquired with mixing times of 30, 60, 100, 150, and 200 ms under the same conditions. The fixed distance of 2.45 Å between C3(H5) and C3(H6) was used as the reference distance. This reference was cross-checked against independent thymine (H6-CH_3) references for residues T5 and T7. A total of 390 distances were obtained for the symmetric menogaril–d(G-A-C-A-T-G-T-C) complex (two drugs per duplex). The distance bounds were as follows: $d < 2.6$ Å, −0.2/+0.3 Å; 2.6 Å < $d < 3.5$ Å, −0.4/+0.5 Å; 3.5 Å < $d < 4.6$ Å, −0.6/+0.7 Å; $d > 4.6$ Å, −0.7/+0.8 Å. For distances involving methyl groups, a 0.3 Å correction was added to the upper bound.[26]

The distance restraints involving exchangeable protons were derived from an 80 ms mixing time NOESY experiment on the complex in H_2O buffer (pH 6.2) at 10 °C. The NOE volumes for all resolved cross peaks were integrated and normalized for the sinusoidal excitation profile. We used the fixed distance of 2.90 Å between A2(H2) and T7(NH3) as the reference distance and derived a total of 58 distance restraints for the symmetric menogaril–d(G-A-C-A-T-G-T-C) complex (two drugs per duplex). The distance restraints were given ±20% bounds, and an additional 0.3 Å upper bound correction was included for NOEs involving methyl protons.[26]

We also included 20 hydrogen bond distance restraints in order to maintain Watson–Crick base pairing alignments during the computations. These distances were derived from known values in crystal structures of oligonucleotides.[27] Two hydrogen bond distances were used for A·T base pairs and three hydrogen bond distances were used for G·C base pairs with a lower and upper bound of 0.1 Å.

NOE volumes at five mixing times were incorporated in the relaxation matrix refinement procedure. The upper and lower bounds for the NOE volumes were estimated in a systematic manner on the basis of the intensities and the minimum detectable NOEs in the spectrum. A total of 2130 intensities estimated at five mixing times (30, 60, 100, 150, and 200 ms) were incorporated in the full relaxation matrix refinement.

Starting Models. Two different starting structures, Init-A and Init-B, were constructed and used for the distance restrained molecular

(20) Plateau, P.; Gueron, M. *J. Am. Chem. Soc.* **1982**, *104*, 7310–7311.
(21) States, D.; Haberkorn, R. A.; Ruben, D. J. *J. Magn. Reson.* **1982**, *48*, 286–292.
(22) Marion, D.; Wuthrich, K. *Biochem. Biophys. Res. Commun.* **1983**, *113*, 967–974.
(23) Bax, A.; Davis, D. G. *J. Magn. Reson.* **1985**, *65*, 355–360.
(24) Griesinger, C.; Otting, G.; Wuthrich, K.; Ernst, R. R. *J. Am. Chem. Soc.* **1988**, *110*, 7870–7872.
(25) Sklenar, V.; Miyashiro, H.; Zon, G.; Miles, H. T.; Bax, A. *FEBS Lett.* **1986**, *208*, 94–98.
(26) Koning, T. M.; Boelens, R.; Kaptein, R. *J. Magn. Reson.* **1990**, *90*, 111–123.
(27) Saenger, W. *Principles of Nucleic Acid Structure*; Springer-Verlag: New York, 1984.

dynamics (MD) calculations. The d(G-A-C-A-T-G-T-C) duplex was generated from standard A- and B-form DNA duplex coordinates in INSIGHT II (Biosym Technologies, Inc.). Intercalation sites were next generated at C3-A4 and T5-G6 steps on both strands. The menogaril molecule was constructed in INSIGHT II on the basis of the crystal structure of nogalamycin in the nogalamycin−d(^{m5}C-G-TsA-^{m5}C-G) complex.[13a] Two menogaril molecules were docked onto the previously built A- and B-form d(G-A-C-A-T-G-T-C) duplexes with the aglycon chromophores intercalated between (C3-A4)·(T5-G6) steps and the bicyclic aminoglucose sugar positioned in the major groove of the DNA. To minimize various bad contacts between menogaril molecules and the DNA, 400 steps of conjugate gradient energy minimization were performed with no NOE restraints on the Init-A (starting from A-form DNA) and Init-B (starting from B-form DNA) starting models of the complex. The root-mean-square deviation (RMSD) was 4.57 Å between Init-A and Init-B and 4.47 Å for the energy-minimized counterparts for all atoms involved.

Distance Restrained Molecular Dynamics Calculations. All the molecular dynamics computations were carried out on a four processor Silicon Graphics Challenge Server using the X-PLOR program.[28] The general procedures for the distance restrained molecular dynamics calculations and relaxation matrix refinement as used in our laboratory have been described previously.[29] The computations were guided by the input distance and intensity restraints derived from the NMR data sets. The molecular dynamics calculations were performed in vacuum with reduced phosphate charges, and a distance-dependent dielectric constant was used to account for the screening effects of solvent and counterions. All the distance restraints were introduced in the form of square-well potentials.

The dynamics were initiated from each energy-minimized starting structure (Init-A and Init-B) with two different seeds for the random number generator that assigns initial velocities from a Maxwellian distribution to every atom in the system. The two energy-minimized starting models were subjected to 400 steps of conjugate gradient energy minimization, in which only the hydrogen bond restraints for the DNA base pairs were kept at a force constant of 20 kcal mol^{-1} Å^{-2}. The initial velocities of all the atoms were assigned on the basis of a Maxwellian distribution at 1000 K. The NOE restraints were introduced gradually over 10 ps (time step of 0.5 fs) during the dynamics at 1000 K with the force constants for restraints in D_2O and in H_2O increased from 1.0 to 20.0 kcal mol^{-1} Å^{-2}. The introduced force constants were then kept constant throughout the subsequent dynamics calculations. After a total of 17 ps of molecular dynamics at 1000 K, the system was slowly cooled to 300 K with retention of the full scale of NOE restraints (time step of 1 fs). The system was subjected to another 8 ps (time step of 1 fs) of restrained molecular dynamics at 300 K. The coordinates during the last 1 ps of dynamics were averaged and energy minimized.

Relaxation Matrix Refinement. The four distance-refined structures were refined further with the relaxation matrix (relax) routine of the X-PLOR program (version 3.0).[28] The NOE intensities (a total of 2130 based on five NOESY data sets collected at mixing times of 30, 60, 100, 150, and 200 ms) were incorporated as a penalty function in the relax energy term, in which exponent $^1/_6$ was used. An isotropic correlation time of 4.4 ns derived from a systematic grid search[30] was used in the computations. The distance-refined structures were subjected to 1 ps of molecular dynamics at 1000 K, during which the scale factors for the NOE intensities were increased from 5 to 200 kcal mol^{-1} and the scale factors for the nonexchangeable proton distance restraints were decreased from 20.0 to 0.0 kcal mol^{-1} Å^{-2}. The scale factors for the hydrogen bond distance restraints and restraints involving exchangeable protons measured in H_2O were retained and were the same as used in the distance restrained molecular dynamics refinement. The scale factors for the NOE intensities were kept at 200 kcal mol^{-1} throughout the refinement procedure. The system was brought down in a slow cooling process from 1000 to 300 K in steps of 50 K. This was followed by 6 ps of molecular dynamics at 300 K with a time step of 1 fs. The coordinates during the last 1 ps of dynamics were averaged, and these averaged coordinates were subjected to 400 steps of energy minimization.

An averaged structure with mean positions for all atoms was computed for the four relaxation matrix refined structures of the complex using X-PLOR.[28] This averaged structure, which was not energy minimized, provides a reference for evaluating the quality and convergence statistics of the four relaxation matrix refined structures of the menogaril−d(G-A-C-A-T-G-T-C) complex.

Structural Analysis. Helical and sugar phosphate backbone parameters were calculated for the four relaxation matrix refined structures of the menogaril−d(G-A-C-A-T-G-T-C) complex using CURVES.[31] The structures were viewed and plotted using INSIGHT II (Biosym Technologies, Inc.).

Results

Menogaril−d(G-A-C-A-T-G-T-C) Complex. The exchangeable proton (6.3−14.5 ppm) and nonexchangeable proton (0.5 to 9.0 ppm) NMR spectra of the menogaril−d(G-A-C-A-T-G-T-C) complex (two drugs per duplex) in 0.1 M NaCl, 10 mM phosphate, and 1 mM EDTA aqueous buffer are shown in the supplementary Figure S1, parts a and b, respectively. We observe proton resonances from a major conformation of the complex along with minor resonances from one or more additional components. The present research focuses on the solution structure of the major conformation of the complex. The 2-fold symmetry of the self-complementary d(G-A-C-A-T-G-T-C) duplex is retained on complex formation with 2 equiv of menogaril. This symmetry is manifested in the observation of a single resonance for the G1, T5, G6, and T7 imino protons of the DNA and a single resonance for the OH-4 and OH-6 hydroxyl protons of the menogaril in the major conformation of the complex (Figure S1a).

Exchangeable DNA Protons. An expanded NOESY (150 ms mixing time) contour plot correlating the imino protons with the base, amino, and imino protons of the menogaril−DNA complex in H_2O buffer at 10 °C is shown in Figure 1a. The most downfield exchangeable proton at 13.66 ppm is assigned to the imino proton of T7 and exhibits an NOE to the H2 proton of A2 (peak B, Figure 1a), establishing formation of Watson−Crick A2·T7 base pairs. The exchangeable proton at 13.09 ppm is assigned to the imino proton of T5 and exhibits a strong cross peak to the superpositioned A4(H2) and A4(NH_2-h) protons (peak C, Figure 1a) and a weaker cross peak to the A4(NH_2-e) proton (peak D, Figure 1a), establishing formation of Watson−Crick A4·T5 base pairs (symbols h and e stand for hydrogen bonded and exposed). The most upfield exchangeable proton at 12.08 ppm is assigned to the imino proton of G6 which exhibits cross peaks to the amino protons of C3 (peaks E and F, Figure 1a), establishing formation of Watson−Crick C3·G6 base pairs. The nucleic acid imino and amino proton chemical shifts in the menogaril−DNA complex at 10 °C are listed in Table 1.

We observed a sequential NOE cross peak between the imino protons of G6 and T7 (peak A, Figure 1a) but not between the imino protons of T5 and G6 in the complex. This suggests that intercalation has occurred at (C3-A4)·(T5-G6) steps in the menogaril−d(G1-A2-C3-A4-T5-G6-T7-C8) complex. We observe extremely weak cross peaks between the imino protons of T5 and G6 and the H_2O resonance (designated by arrows), indicative of slow exchange between these imino protons and solvent in the complex.

Exchangeable Menogaril Protons. Expanded NOESY (150 ms mixing time) contour plots correlating the menogaril

(28) Brunger, A. T. X-PLOR version 3.0. Yale University, CT, 1992.
(29) Chen, H.; Patel, D. J. *J. Mol. Biol.* **1995**, *246*, 164−179.
(30) Nilges, M.; Habazettl, J.; Brunger, A. T.; Holak, T. A. *J. Mol. Biol.* **1991**, *219*, 499−510.
(31) (a) Lavery, R.; Sklenar, H. *J. Biomol. Struct. Dyn.* **1988**, *6*, 63−91. (b) Lavery, R.; Sklenar, H. *J. Biomol. Struct. Dyn.* **1989**, *6*, 655−667.

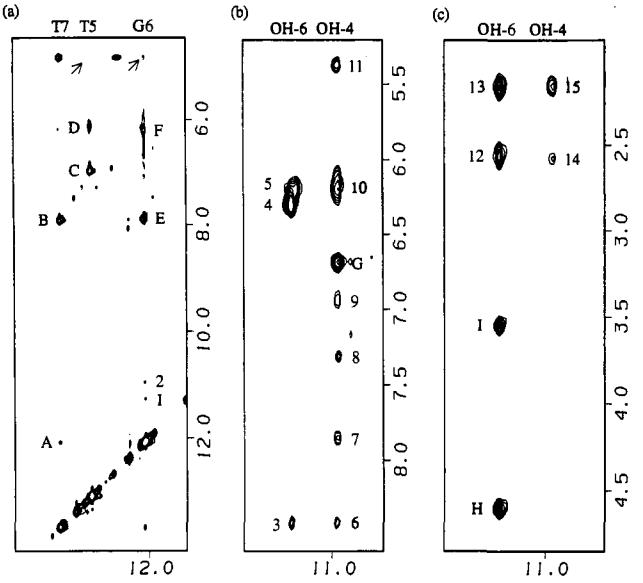

Figure 1. Expanded NOESY (150 ms mixing time) contour plots of the menogaril–d(G-A-C-A-T-G-T-C) complex (two drugs per duplex) in H_2O buffer (pH 6.2) at 10 °C. (a) Distance connectivities correlating the imino protons (11.3–14.5 ppm) with the base, amino, and imino protons (4.5–14.1 ppm). The intermolecular NOE cross peaks 1 and 2 are assigned as follows. 1: G6(NH1)–M(OH-6); 2: G6(NH1)–M(OH-4). The cross peaks A–F are assigned as follows. A: T7(NH3)–G6-(NH1); B: T7(NH3)–A2(H2); C: T5(NH3)–A4(H2/NH_2-h); D: T5(NH3)–A4(NH_2-e); E: G6(NH1)–C3(NH_2-h); F: G6(NH1)–C3-(NH_2-e). The exchange peaks between the T5(NH3) and G6(NH1) protons and the H_2O resonance are absent or very weak in the complex and are designated by arrows. (b) Distance connectivities correlating the menogaril hydroxyl protons (10.6–11.6 ppm) and the base and amino protons (5.2–8.6 ppm). The intermolecular NOE cross peaks 3–11 are assigned as follows. 3: M(OH-6)–A4(H8); 4: M(OH-6)–A4(H1′); 5: M(OH-6)–C3(H1′); 6: M(OH-4)–A4(H8); 7: M(OH-4)–C3(NH_2-h); 8: M(OH-4)–C3(H6); 9: M(OH-4)–A4(NH_2-h); 10: M(OH-4)–C3(NH_2-e)/A4(NH_2-e); 11: M(OH-4)–C3(H5). NOE cross peak G is assigned to M(OH-4)–M(H3). (c) Distance connectivities correlating the menogaril hydroxyl protons (10.6–11.6 ppm) and the sugar protons (1.9–4.9 ppm). The intermolecular NOE cross peaks 12–15 are assigned as follows. 12: M(OH-6)–C3(H2″)/A4(H2″); 13: M(OH-6)–C3(H2′)/A4(H2′); 14: M(OH-4)–C3(H2″); 15: M(OH-4)–C3(H2′). NOE cross peaks H and I are assigned as follows. H: M(OH-6)–M(H7); I: M(OH-6)–M(OCH_3-7).

hydroxyl protons with the base and amino protons and with the sugar protons in the menogaril–DNA complex in H_2O buffer at 10 °C are shown in Figure 1, parts b and c, respectively. The 11.27 ppm exchangeable proton is assigned to the OH-6 menogaril proton on the basis of NOEs to the H7 (peak H, Figure 1c) and OCH_3-7 (peak I, Figure 1c) menogaril protons in the complex. The 10.96 ppm exchangeable proton is assigned to the OH-4 menogaril proton on the basis of the NOE to the H3 menogaril proton (peak G, Figure 1b) in the complex. The menogaril hydroxyl proton chemical shifts in the menogaril–DNA complex at 10 °C are listed in Table 2.

Nonexchangeable DNA Protons. The expanded NOESY (250 ms mixing time) contour plot correlating the base proton region (6.5–8.6 ppm) with the sugar H1′ and H3′ proton region (4.3–6.5 ppm) of the complex in D_2O buffer at 25 °C is plotted in Figure 2. The NOE connectivities between the base (pyrimidine H6 and purine H8) protons and their own and 5′-flanking sugar H1′ (and H3′) protons can be traced from G1 to C8 in the d(G1-A2-C3-A4-T5-G6-T7-C8) sequence in the complex (Figure 2). The NOEs between the base proton and the H1′ (and H3′) protons are very weak for the T5-G6 step (see arrows, Figure 2) suggestive of intercalation of menogaril at this step in the complex. We do detect the NOEs between the base proton and the H1′ (and H3′) protons for the C3-A4 step (Figure 2) in the complex. This suggests that the (C3-A4)•(T5-G6) intercalation site may be wedged-shaped with a greater separation between T5 and G6 relative to between C3 and A4 in the complex.

The base and sugar nucleic acid nonexchangeable proton assignments in the menogaril–DNA complex at 25 °C listed in Table 1 are based on an analysis of the entire NOESY spectrum, and the assignments were confirmed following an analysis of DQF-COSY and TOCSY spectra.

The nucleic acid complexation chemical shifts on proceeding from the d(G-A-C-A-T-G-T-C) duplex to the menogaril–d(G-A-C-A-T-G-T-C) complex (two drugs per duplex) are listed in supplementary Table S1. We detect upfield shifts at the NH_2-h (−0.64 ppm) and H2 (−0.52 ppm) base protons and H2′,2″ (−0.40, −0.38 ppm) sugar protons of A4 and downfield shifts at the H1′ (0.44 ppm) and H2′,2″ (0.33, 0.35 ppm) sugar protons of T5 on formation of the menogaril–DNA complex (Table S1).

We observe strong NOEs between the base and their own sugar H3′ protons for residues C3, A4, and C8 in the 250 ms mixing time expanded NOESY contour plot of the complex in D_2O at 25 °C in Figure 2. The relative intensities of these base to H3′ proton NOEs can be compared to the intensity of the cytidine H6 to H5 NOE (fixed distance of 2.45 Å) for the residue labeled C3* in an expanded stacked plot of a shorter mixing time (60 ms) NOESY spectrum plotted in supplementary Figure S2a. A short base to its own sugar H3′ proton separation reflected in a strong NOE between these protons is characteristic of a C3′-*endo* sugar pucker family. These data establish that the sugar puckers of C3, A4, and C8 in the menogaril–DNA complex are not in the C2′-*endo* deoxy sugar pucker range but instead approach the C3′-*endo* sugar pucker range.

An expanded DQF-COSY contour plot correlating coupling connectivities between sugar H1′ and H3′ protons and the sugar H2′,2″ protons in the menogaril–DNA complex in D_2O buffer at 25 °C is plotted in supplementary Figure S2b. We observe resolved H2′,2″ protons for C3 and A4 while those for C8 are superpositioned on each other. We note that the H1′ proton of A4 exhibits a coupling cross peak to its own H2″ but not H2′ proton while the H3′ proton of A4 exhibits coupling cross peaks to its own H2′ and H2″ protons (Figure S2b). Such coupling patterns are characteristic of a C3′-*endo* pucker geometry for A4 in the complex.

Nonexchangeable Menogaril Protons. The nonexchangeable menogaril protons were assigned following analysis of the NOESY, DQF-COSY, and TOCSY spectra of the menogaril–DNA complex in D_2O at 25 °C. Thus, the bicyclic aminoglucose sugar protons were assigned starting from the aglycon H3 proton (6.69 ppm) and proceeding via an NOE to the bicyclic aminoglucose sugar CH_3-5″ protons and subsequently to the H1″ proton at the other end via sequential through-space and through-bond connectivities. The aglycon ring A geminal H10a,b protons (2.84 and 2.94 ppm) were distinguished from the geminal H8a,b protons (2.30 and 2.03 ppm) since the former exhibit an NOE to the 6.83 ppm H11 proton while the latter exhibit NOE and coupling cross peaks (peaks A and B, Figure S2b) to the 4.61 ppm H7 proton in the menogaril molecule. The nonexchangeable menogaril proton chemical shifts in the menogaril–DNA complex at 25 °C are listed in Table 2.

Phosphorus Chemical Shifts and Assignments. The proton decoupled phosphorus spectrum of the menogaril–d(G-A-C-

Table 1. Nucleic Acid Proton Chemical Shifts for the Menogaril–d(G-A-C-A-T-G-T-C) Complex[a]

	chemical shifts (ppm)									
residue	NH	NH_2	H8/H6	H2/H5/CH_3	H1′	H2′	H2″	H3′	H4′	$^{31}P^b$
G1	12.60		7.85		5.67	2.50	2.66	4.80	4.16	−4.06
A2			8.16		6.18	2.55	2.78	5.03	4.35	−3.77
C3		7.84, 6.20	7.32	5.37	6.23	2.16	2.57	4.92	4.18	−4.40
A4		6.98, 6.12	8.41	6.99	6.31	2.20	2.52	4.78	4.22	−4.48
T5	13.09		7.38	1.32	6.17	2.40	2.74	4.97	4.31	−3.76
G6	12.08		7.81		5.61	2.48	2.62	4.91	4.44	−4.34
T7	13.66		7.14	1.11	5.97	2.10	2.41	4.81	4.13	−3.92
C8			7.57	5.65	6.23	2.23	2.23	4.51	4.01	

[a] Buffer solution contains 0.1 M NaCl, 10 mM phosphate, and 1 mM EDTA. The nonexchangeable proton data were obtained in D_2O (pH 6.2) at 25 °C. The exchangeable proton data were obtained in H_2O (pH 6.2) at 10 °C. [b] ^{31}P chemical shifts correspond to residues (*n*) in the (*n*)-^{31}P-(*n*+1) step.

Table 2. Menogaril Proton Chemical Shifts (ppm) for the Menogaril–d(G-A-C-A-T-G-T-C) Complex (Two Drugs per Duplex)[a]

aglycon ring		bicyclic aminoglucose sugar	
proton	shift	proton	shift
H3	6.69	H1″	5.23
OH-4	10.96	H2″	4.05
OH-6	11.27	H3″	4.44
H7	4.61	$N(CH_3)_2$-3″a	2.30
OCH_3-7	3.55	$N(CH_3)_2$-3″b	2.86
H8a	2.30	H4″	3.79
H8b	2.03	CH_3-5″	1.49
CH_3-9	1.34		
H10a	2.84		
H10b	2.94		
H11	6.83		

[a] Buffer solution contains 0.1 M NaCl, 10 mM phosphate, and 1 mM EDTA. The nonexchangeable proton data were obtained in D_2O (pH 6.2) at 25 °C. The exchangeable proton data were obtained in H_2O (pH 6.2) at 10 °C.

A-T-G-T-C) complex in D_2O buffer (pH 6.2) at 25 °C exhibits three phosphorus resonances slightly downfield of the −4.0 to −4.5 ppm range characteristic of unperturbed phosphodiester backbones. These phosphorus resonances have been assigned to the T7-C8 (−3.92 ppm), the A2-C3 (−3.77 ppm), and the T5-G6 (−3.76 ppm) steps in the menogaril–d(G1-A2-C3-A4-T5-G6-T7-C8) complex following analysis of a proton-detected proton–phosphorus correlation experiment (supplementary Figure S3). The phosphorus chemical shifts in the menogaril–DNA complex at 25 °C are listed in Table 1.

Intermolecular Interactions. We observe a large number of intermolecular NOEs between the menogaril and the DNA (Table 3) that define the intermolecular interactions associated with complex formation. The NOEs identify the intercalation site, the relative alignment between the intercalated aglycon of menogaril and the flanking base pairs, as well as the interactions between the bicyclic aminoglucose sugar and the DNA groove at the binding site.

The OH-4 and OH-6 hydroxyl protons along one long edge of the aglycon ring **3** exhibit a large number of intermolecular NOEs to the base and sugar protons of C3 and A4 in the menogaril–DNA complex (Table 3 and Figure 1b,c). Thus, the OH-4 proton exhibits intermolecular NOEs to the major groove H5 and H6 (peaks 11 and 8, respectively, Figure 1b) and the NH_2-h and NH_2-e (peaks 7 and 10, respectively, Figure 1b) base protons of C3 and the major groove H8 proton of A4 (peak 6, Figure 1b). These intermolecular NOEs position the OH-4 proton of the intercalated aglycon ring toward the major groove edge of the C3-A4 step at the intercalation site. The OH-6 proton exhibits NOEs to the minor groove H1′ (peak 5, Figure 1b) and H2′ and H2″ (peaks 13 and 12, respectively, Figure 1b) sugar protons of C3 and the H1′ sugar proton of A4

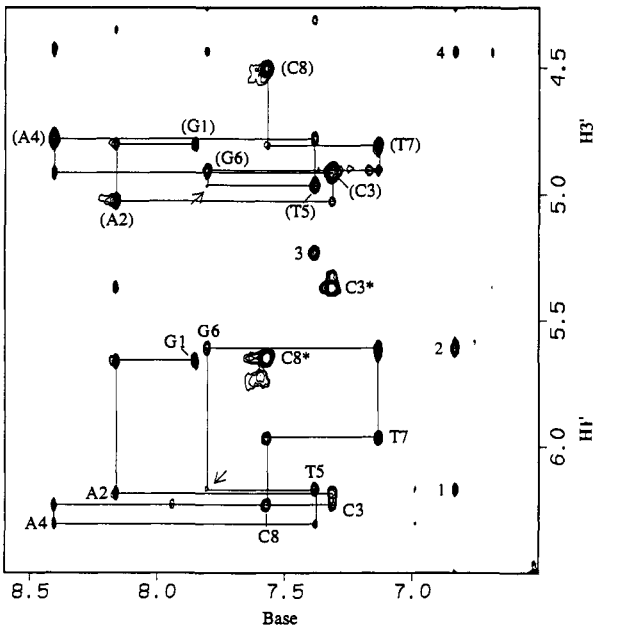

Figure 2. Expanded NOESY (250 ms mixing time) contour plot correlating the base protons (6.5–8.6 ppm) and the sugar H1′ and H3′ protons (4.3–6.5 ppm) of menogaril–d(G-A-C-A-T-G-T-C) complex in D_2O buffer solution (pH 6.2) at 25 °C. The two C(H5-H6) cross peaks for C3 and C8 are designated by asterisks. The NOE connectivities between the base and their own and 5′-flanking sugar H1′ protons (5.6–6.4 ppm) and H3′ protons (4.5–5.1 ppm) are traced from G1 to C8. The missing or very weak cross peaks at the T5-G6 steps are designated by arrows. The intermolecular NOE cross peaks 1–4 are assigned as follows. 1: M(H11)–T5(H1′); 2: M(H11)–G6(H1′); 3: M(H1″)–T5(H6); 4: M(H11)–G6(H4′).

(peak 4, Figure 1b). These intermolecular NOEs position the OH-6 proton of the intercalated aglycon ring toward the minor groove edge of the C3-A4 step at the intercalation site. These results require not only that the OH-4- and OH-6-containing long edge of the intercalated aglycon ring be directed toward the C3-A4 step but also that it be aligned with its long axis orthogonal to the long axis of the flanking C3·G6 and A4·T5 base pairs. Further, the intermolecular NOE data require that the bicyclic aminoglucose sugar which is adjacent to OH-4 be positioned in the major groove while the nonplanar cyclohexene ring A of the aglycon be positioned in the minor groove in the menogaril–DNA complex. This alignment of the aglycon at the intercalation site is reinforced by the intermolecular NOEs between the H11 proton located on the other long edge of the aglycon and the minor groove H1′ proton of T5 (peak 1, Figure 2) and the H1′ and H4′ protons of G6 (peaks 2 and 4, respectively, Figure 2) in the menogaril–DNA complex.

The H7, OCH_3-7, CH_3-9, and H10a,b protons on ring A of the aglycon exhibit a large number of intermolecular NOEs to

Table 3. Intermolecular NOEs between Menogaril Protons and DNA Protons in the Menogaril–d(G-A-C-A-T-G-T-C) Complex (Two Drugs per Duplex)

menogaril protons	DNA protons		
	minor groove	helix axis	major groove
H3		G6(NH3)	C3(H5, NH_2-h,e)
OH-4	C3(H2′, H2″)	G6(NH3)	C3(H5, H6, NH_2-h,e); A4(H8, NH_2-h,e)
OH-6	C3(H1′, H2′, H2″); A4(H1′)	G6(NH3)	A4(H8)
H11	A4(H2); T5(H1′); G6(H1′, H4′, H5′, H5″)		G6(H8)
H7	A4(H1′)		
OCH_3-7	A4(H1′, H2′, H2″, H4′)		
CH_3-9	G6(H1′, H2″, H4′); T7(H4′)		
H10a	G6(H1′)		
H10b	G6(H1′)		
H1″	T5(H2′, H2″, H3′)		T5(CH_3, H6)
H2″			T5(CH_3)
$N(CH_3)_2$-3″a			T7(CH_3)
$N(CH_3)_2$-3″b			T7(CH_3)

the minor groove sugar H1′, H2″, and H4′ protons of A4 and G6 of the (C3-A4)•(T5-G6) intercalation site in the complex (Table 3). The distribution of these intermolecular NOEs require the C7-containing edge of aglycon ring A be closer to A4 while the C10-containing edge be closer to G6, thus positioning the aglycon nonplanar cyclohexene ring A in the middle of the minor groove in the complex.

The bicyclic aminoglucose sugar H1″ proton exhibits NOEs to the major groove H6 and CH_3 base and H3′ sugar protons of T5 in one direction while the $N(CH_3)_2$-3″a,b protons exhibit NOEs to the major groove CH_3 protons of T7 in the opposite direction in the T5-G6-T7 segment. These intermolecular NOEs define the alignment of the bicyclic aminoglucose sugar in the major groove of the complex.

Distribution of Restraints. The cross peaks in the NOESY data sets of the menogaril–d(G-A-C-A-T-G-T-C) complex in H_2O and D_2O buffer solutions are sufficiently well resolved to permit quantitation of the experimental NMR data to deduce restraints to guide the structure calculations. The procedures used to estimate the magnitude and bounds for the exchangeable, nonexchangeable, and hydrogen bond distance restraints in the menogaril–DNA complex are outlined in the Experimental Section. These restraints are summarized graphically on the basis of the number and type at each residue in the complex. The distribution between nonexchangeable (open rectangles), exchangeable (closed rectangles), and hydrogen bond (hatched rectangles) restraints within individual nucleic acid residues and within the drug molecule in the complex are plotted in Figure 3a. We have also plotted the distribution between intraresidue (open rectangles) and interresidue (closed rectangles) distance restraints within individual nucleic acid residues and within the drug molecule for the complex in Figure 3b. The distribution of exchangeable (open rectangles) and nonexchangeable (closed rectangles) intermolecular restraints between menogaril and DNA protons in the complex are outlined in Figure 3c. These intermolecular restraints are centered about the (C3-A4-T5-G6)•(C3-A4-T5-G6) segment which encompasses the two symmetry-related menogaril binding sites. The intraresidue restraints were counted as one for the residue while each interresidue or drug–DNA restraint was counted as one-half for that residue and one-half for its partner in the interaction. The molecular dynamics calculations were guided by 318 DNA–DNA restraints, 72

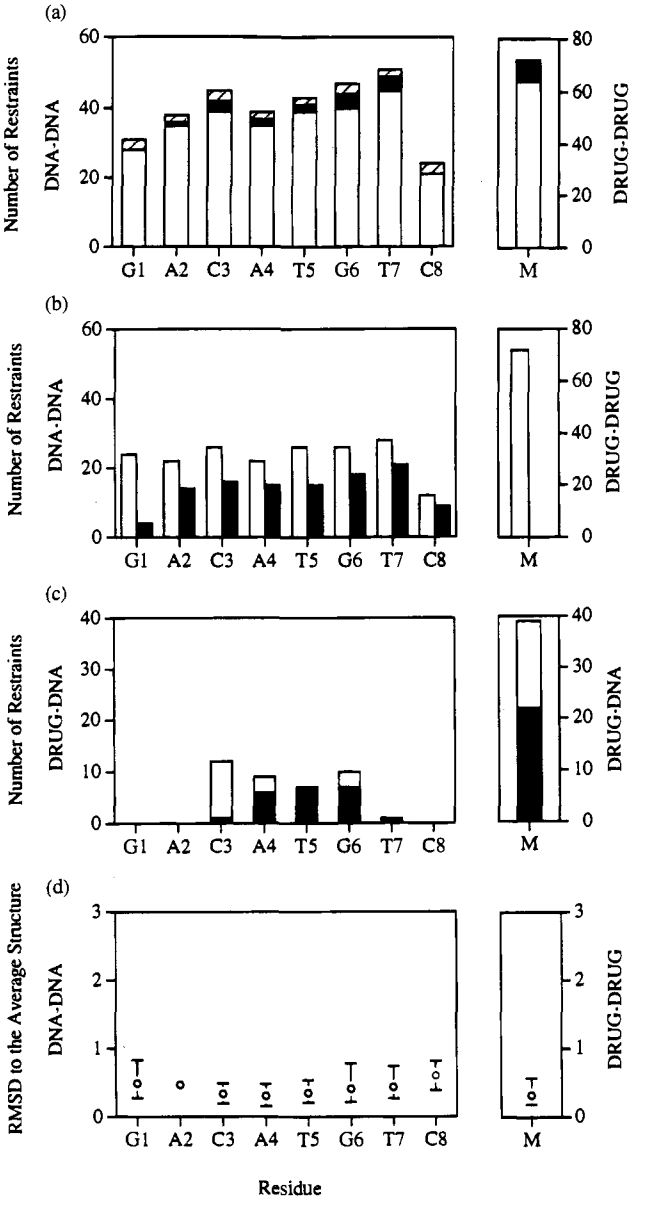

Figure 3. Distribution of restraints for individual nucleic acid residues and the drug molecules in the structure calculation of the menogaril–d(G-A-C-A-T-G-T-C) complex. (a) Restraints have been classified as follows: nonexchangeable proton restraints (open rectangles) that were calculated on the basis of NOE buildups in D_2O, exchangeable proton restraints (filled rectangles) that were calculated from the NOESY spectrum in H_2O, and hydrogen bond restraints (hatched rectangles) used to maintain base pairing. Each intraresidue restraint is counted as one for that residue. Each interresidue restraint is counted as one-half for that residue and one-half for its partner in the interaction. The left panel lists DNA–DNA restraints for individual residues, and the right panel lists drug–drug restraints. (b) Distribution by residue of intraresidue (open rectangles) and interresidue (filled rectangles) experimentally observed exchangeable proton and nonexchangeable proton restraints. The DNA–DNA NOEs are shown in left panel and drug–drug NOEs in the right panel. (c) Intermolecular drug–DNA NOEs of exchangeable protons (open rectangles) and nonexchangeable protons (filled rectangles) involving specific DNA residues (left panel) and the drug molecule (right panel). Each intermolecular restraint is counted as one-half for that residue and one-half for its partner in the interaction. (d) Pairwise RMSDs in the atomic coordinate positions calculated for each nucleic acid residue (left panel) and drug molecule (right panel) between the four relaxation-refined structures and the averaged structure of the complex. The average values (open circles) are shown along with extreme values (vertical bars).

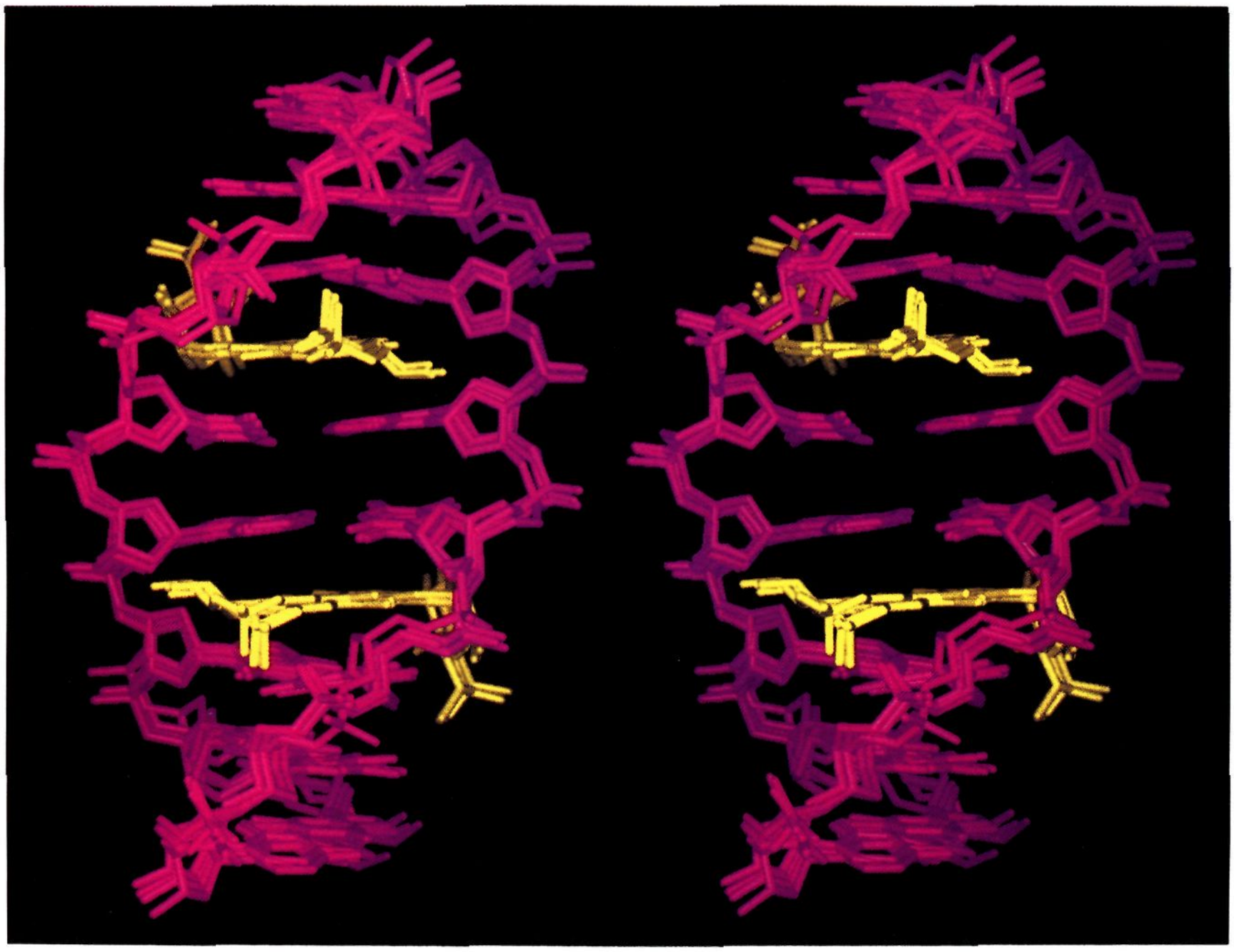

Figure 4. Stereoviews of four superpositioned relaxation matrix refined structures of the menogaril−d(G-A-C-A-T-G-T-C) complex (two drugs per duplex). The menogaril is in yellow, and the DNA duplex is in magenta. The view is looking into the minor groove.

Table 4. NMR Refinement Statistics

Starting Structures	
pairwise RMSD between the starting structures Init-A and Init-B[a]	4.57
Distance Refinement	
no. of distance restraints	468
NOE violations (>0.2 Å) for the four distance-refined structures	13−18
RMSDs for the input distance restraints in the four distance-refined structures	0.067−0.070
pairwise RMSDs among the four distance-refined structures[a]	0.56−0.90
Relaxation Matrix Refinement	
no. of intensity restraints (total of five mixing times)	2130
no. of distance restraints involving exchangeable protons[b]	78
NOE violations (>0.2 Å) for the four relaxation matrix refined structures	2
RMSDs for the input distance restraints in the four relaxation matrix refined structures[b]	0.069−0.070
pairwise RMSDs among the four relaxation matrix refined structures[a]	0.64−0.90

[a] RMSDs were calculated for all eight base pairs of the DNA and the two menogaril molecules in the menogaril−d(G-A-C-A-T-G-T-C) complex. [b] These NOE violations and RMSDs for input distance restraints are restricted to the 78 exchangeable protons and hydrogen bonding distance restraints that were used during relaxation matrix refinement.

drug−drug restraints, and 78 drug−DNA restraints for the menogaril−d(G-A-C-A-T-G-T-C) complex (two drugs per duplex).

Table 5. Quality of Structures for the Menogaril−d(G-A-C-A-T-G-T-C) Complex

parameter	initial structures	distance-restrained MD structures	relaxation matrix MD structures
RMSD Values from Ideal Covalent Geometry			
bond length (Å)	0.007−0.009	0.010−0.011	0.011−0.012
bond angles (deg)	3.348−3.432	3.350−3.417	3.684−3.833
impropers (deg)	0.170−0.238	0.221−0.284	0.219−0.286
R Factors[a]			
unweighted R_1	0.544−0.620	0.351−0.364	0.238−0.263
weighted R_1	1.048−1.126	0.456−0.471	0.382−0.440
$R_{1/6}$	0.080−0.113	0.052−0.054	0.036−0.039
Convergence			
RMSD values relative to averaged structure (Å)[b]	1.60−3.11	0.85−1.03	0.36−0.46

[a] The definitions for the various *R* factors are taken from ref 30. [b] RMSD values are relative to the average of the four final structures of the complex containing all eight base pairs and the two drug molecules.

Structure Calculations. The NOE information was quantitated and converted into distance restraints as described in the Experimental Section, and these were then used to calculate structures using the restrained molecular dynamics module in the X-PLOR program. The two starting structures Init-A and Init-B (RMSD = 4.57 Å) were generated as described in the Experimental Section. The protocol for the distance-restrained molecular dynamics simulation are outlined in the Experimental

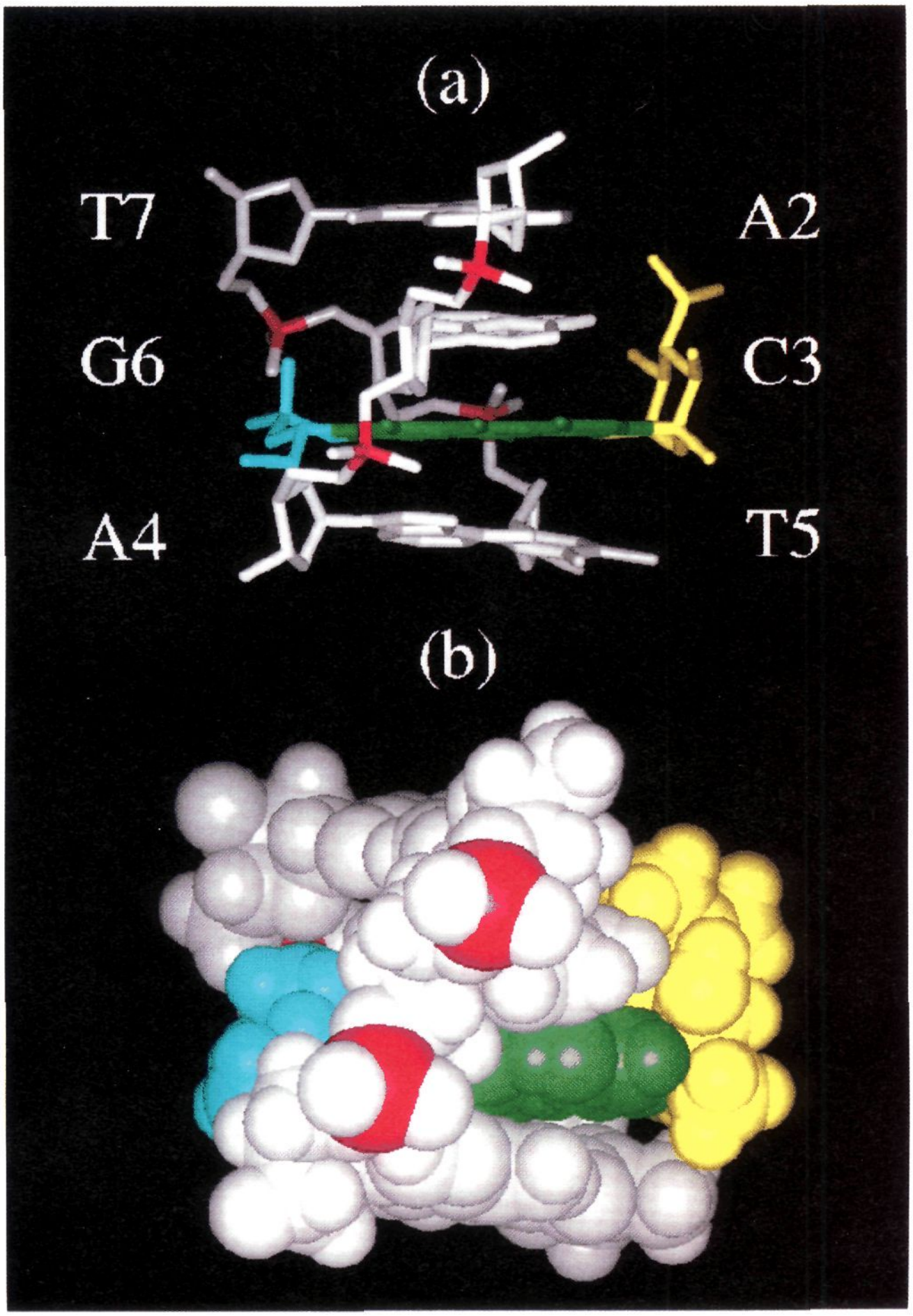

Figure 5. (a) Stick view normal to the helix axis of the menogaril–d(A2-C3-A4)·d(T5-G6-T7) segment in one representative relaxation matrix refined structure of the menogaril–d(G-A-C-A-T-G-T-C) complex (two drugs per duplex). Menogaril aromatic rings B, C, and D of the aglycon are in green, nonplanar cyclohexene ring A of the aglycon is in blue, and the bicyclic aminoglucose sugar is in yellow. The DNA is in white with the backbone phosphorus in red. (b) Corresponding space filling view of the menogaril–d(A2-C3-A4)·d(T5-G6-T7) segment of the complex.

Section. The dynamics were initiated with two different seeds for the random number generator which assigns initial velocities from a Maxwellian distribution to every atom in the system. The calculations yielded four distance-refined structures with pairwise RMSDs of 0.56–0.90 Å for the eight base pairs and the two drug molecules. These structures were next refined against the nonexchangeable proton NOE intensities while retaining the exchangeable proton distance restraints with the protocols for the relaxation matrix refinement outlined in the Experimental Section. The calculations yielded four intensity-refined structures with pairwise RMSDs of 0.64–0.90 Å for the same segment of the complex. Stereoviews of the four superpositioned relaxation matrix refined structures of the menogaril–DNA complex (two drugs per duplex) are plotted in Figure 4. The distribution of pairwise RMSDs in the atomic coordinate positions calculated for each nucleic acid residue and drug molecule among the four relaxation matrix refined structures of the complex is outlined in Figure 3d. The relevant refinement statistics on the menogaril–DNA complex are summarized in Table 4. The qualities of structures of the complex as judged by the *R* factors and deviations from ideal covalent geometry are listed in Table 5.

Structural Features. Both the drug and the DNA are well defined in the relaxation matrix refined structures of the menogaril–d(G-A-C-A-T-G-T-C) complex (two drugs per duplex) (Figure 4). Individual menogarils intercalate at the

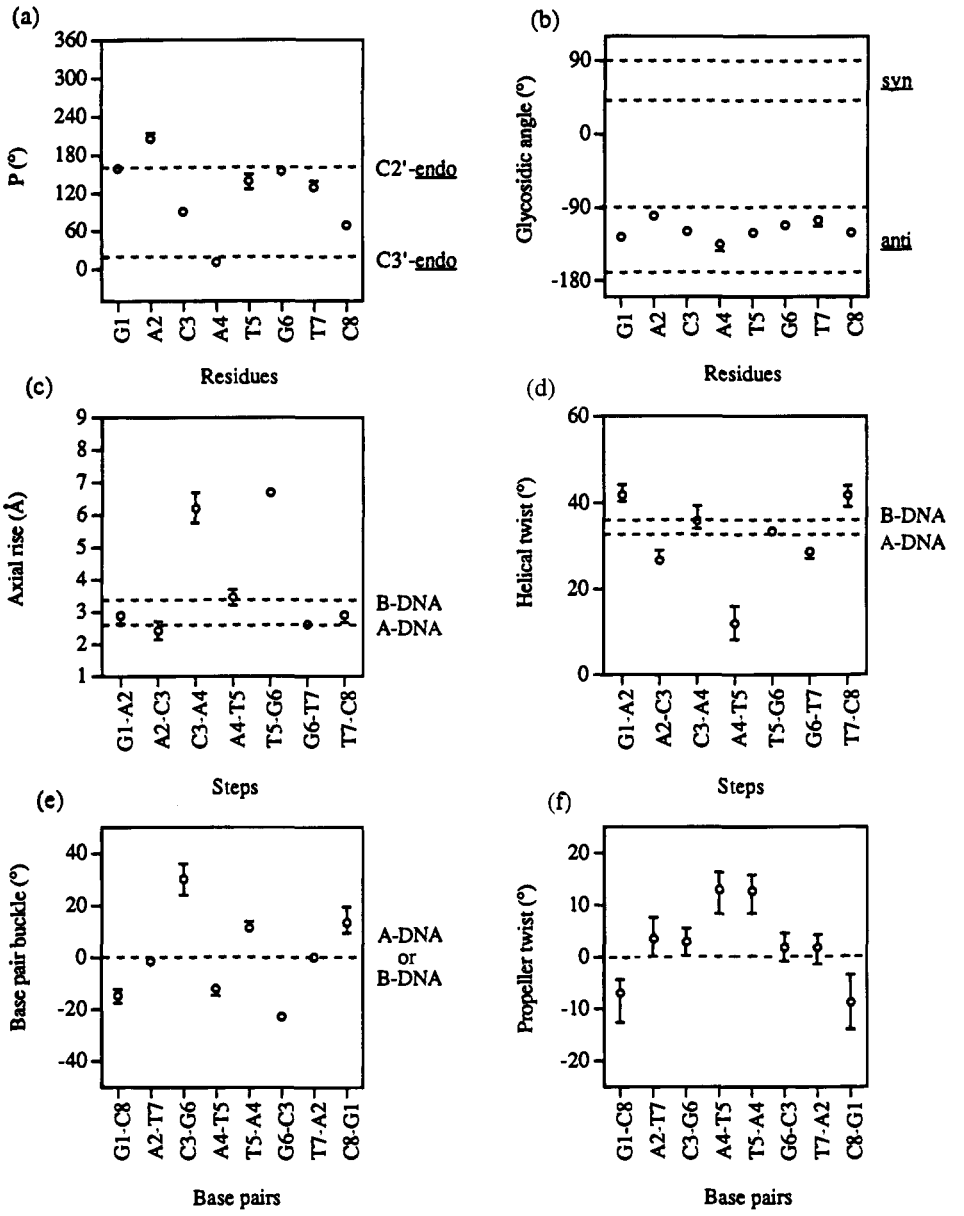

Figure 6. Helical parameters deduced using the CURVES program for the menogaril–d(G-A-C-A-T-G-T-C) complex (two drugs per duplex). (a) Pseudorotation angles for sugar rings and (b) glycosidic torsion angles at individual residues in the complex. (c) Axial rise and (d) helical twist at individual steps in the complex. (e) Base pair buckle and (f) propeller twist for each base pair in the complex. The circle represents the average value, while the spread in values for the four refined structures is represented by lower and upper bounds.

symmetry-related (C3-A4)•(T5-G6) steps on the self-complementary d(G1-A2-C3-A4-T5-G6-T7-C8) duplex with retention of 2-fold symmetry on complex formation. A view of the (A2-C3-A4)•(T5-G6-T7) segment with menogaril intercalated between C3•G6 and A4•T5 base pairs in one representative relaxation matrix refined structure is shown in a stick representation in Figure 5a and in a space filling representation in Figure 5b. The aglycon threads the DNA helix at its intercalation site with its nonplanar cyclohexene ring A (in blue, Figure 5a) positioned in the minor groove and the bicyclic aminoglucose sugar (in yellow, Figure 5a) positioned in the major groove with its $N(CH_3)_2$-3″ charged side chain directed toward the C3•G6 base pair. The DNA duplex is right-handed in the complex with all base pairs retaining Watson–Crick alignment. The various helical parameters for the DNA segment in the four relaxation matrix refined structures of the menogaril–DNA complex are plotted in Figure 6a–f. The stacking pattern between the intercalated aglycon and the flanking C3•G6 and A4•T5 base pairs in one representative relaxation matrix refined structure is shown in stereoview in Figure 7b, along with the stacking patterns between the adjacent A2•T7 and C3•G6 base pairs in Figure 7a and between symmetry-related A4•T5 base pairs in Figure 7c. The sequence specificity of complex formation is associated, in part, with an intermolecular hydrogen bond between the OH-2″ of menogaril and N7 of G6 in the major groove (Figure 8b and Table 6). In addition, an intermolecular hydrogen bond is detected between the OH-9 of menogaril and O2P of the G6-T7 step in the minor groove (Figure 8a and Table 6).

Discussion

Complex Formation and Binding Cooperativity. The structure analysis was facilitated by the formation of a predominant symmetrical complex involving two menogarils bound per self-complementary d(G-A-C-A-T-G-T-C) duplex (Figure S1a,b). We detected 2:1 but not 1:1 complexes of menogaril and the d(G-A-C-A-T-G-T-C) duplex on gradual addition of the drug to the DNA oligomer in solution. This establishes that the two menogarils bind cooperatively to the d(G-A-C-A-T-G-T-C) duplex.

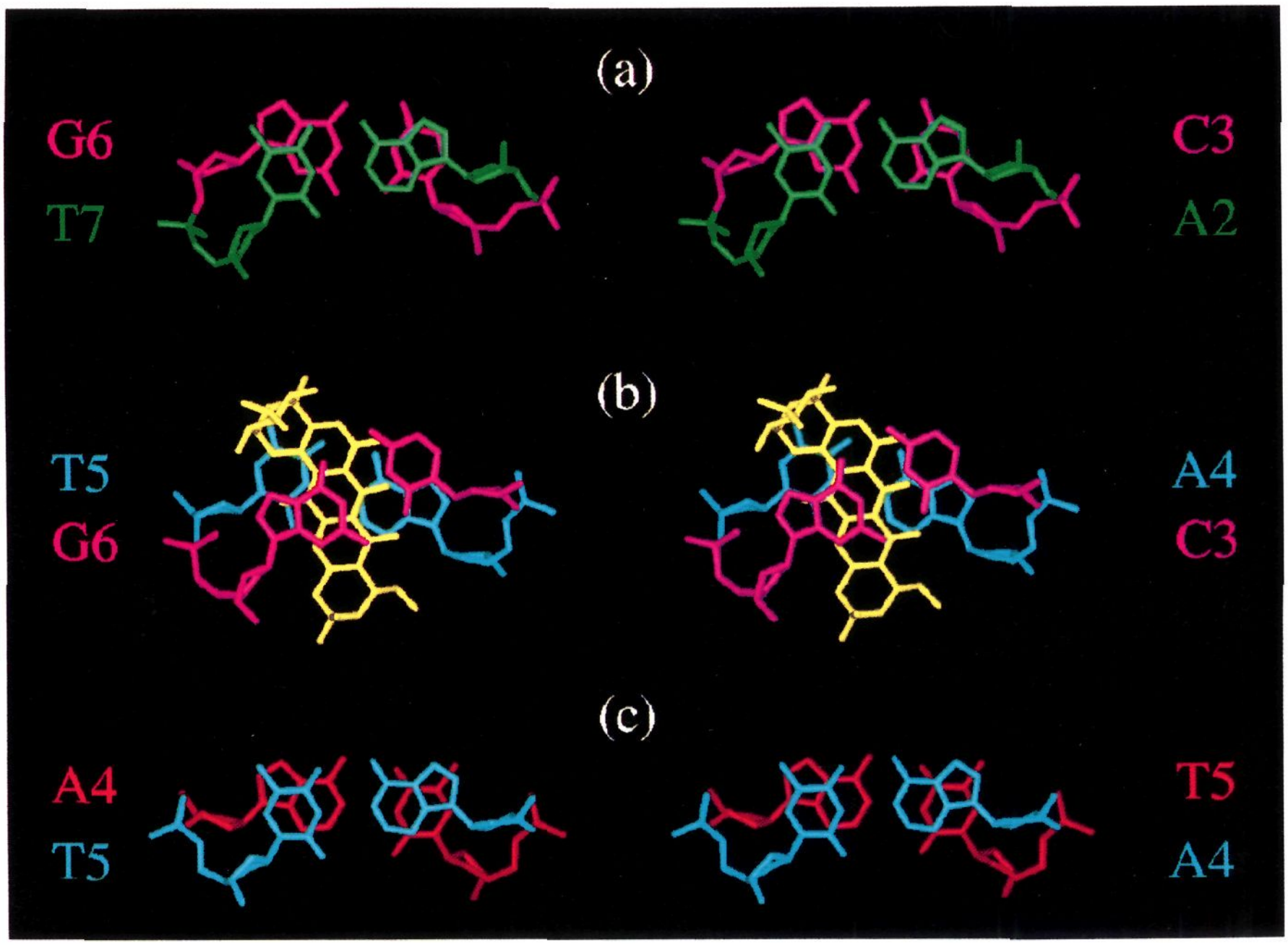

Figure 7. Stereoviews of overlap geometries at individual steps in one representative relaxation matrix refined structure of the menogaril–d(G-A-C-A-T-G-T-C) complex (two drugs per duplex). (a) Overlap between the A2·T7 (in green) and C3·G6 (in magenta) base pairs. (b) Overlap between the aglycon of the intercalated menogaril (in yellow) and flanking C3·G6 (in magenta) and A4·T5 (in blue) base pairs. (c) Overlap between symmetry-related A4·T5 (in blue and red) base pairs in the center of the complex.

NMR Spectral Quality and Solution Structures. The menogaril (Table 2) and DNA (Table 1) proton assignments could be readily made by following analysis of the NOESY data sets on the menogaril–d(G-A-C-A-T-G-T-C) complex (two drugs per duplex). These experimental studies also yielded the intermolecular NOE based restraints (Table 3) which served as input parameters for molecular dynamics calculations guided initially by distance restraints and subsequently by intensity restraints.

The pairwise RMSD's of 4.57 Å between the two starting structures of the complex fell to values between 0.64 and 0.90 Å for the four relaxation matrix refined structures (Table 4). Similarly, the $R_{1/6}$ factor decreased from values of 0.080–0.113 for the starting structures to values of 0.036–0.039 for the relaxation matrix refined structures of the complex (Table 5). *Menogaril intercalates at symmetry-related (C3-A4)·(T5-G6)* steps, and this internal segment is extremely well defined in the complex (Figure 4).

The DNA duplex is right-handed with Watson–Crick pairing (Figure 7) and *anti* glycosidic torsion angles (Figure 6b) at all base pairs in the complex. The DNA helix axis passes through the base pairs (X displacement $\sim$ 0 Å) in the complex, a feature characteristic of the B–DNA family of helixes.

Intercalation Site. Menogaril intercalates at symmetry-related (C3-A4)·(T5-G6) steps separated by the central (A4-T5)·(A4-T5) step in the d(G1-A2-C3-A4-T5-G6-T7-C8) duplex (Figure 4). The long axis of the aglycon is normal to the long axis of the flanking base pairs with the cyclohexene ring A of the aglycon positioned in the minor groove and the bicyclic aminoglucose sugar positioned in the major groove (Figure 7b). The (C3-A4)·(T5-G6) intercalation site is wedged-shaped (Figure 8) with the extent of buckling greater at the C3·G6 base pair than at the A4·T5 base pair (Figure 6e). The axial rise is somewhat greater at the T5-G6 step compared to the C3-A4 step (Figure 6c), and this may explain the break in the NOE connectivities between the base proton and its 5′-flanking sugar H1′ and H3′ protons observed for the T5-G6 but not C3-A4 steps in the complex (Figure 2). The sugar pucker of A4 is C3′-*endo* (P = 11°) while that of G6 is C2′-*endo* (P = 151°) (Figure 6a), consistent with the observed pattern of base to H3′ NOE intensities (Figure S2a) and sugar proton coupling connectivities (Figure S2b) for these residues in the complex.

The B and C aromatic rings of the intercalated aglycon stack primarily with G6 in the complex with the OH-4/OH-6 bearing edge of the aglycon directed toward the C3-A4 strand (Figure 7b). Interestingly, no unwinding is detected at the (C3-A4)·(T5-G6) intercalation step in the complex (Figure 6d).

Steps Flanking the Intercalation Site. Intercalation of menogaril at (C3-A4)·(T5-G6) steps in the d(G-A-C-A-T-G-T-C) duplex results in unwinding at base pair steps flanking the intercalation site. We observe a helical twist of 12° (Figure 6d) corresponding to an unwinding of 24° between the central (A4-T5)·(A4-T5) step in the complex. By contrast, the helical twist values are ~27° (Figure 6d), corresponding to a smaller

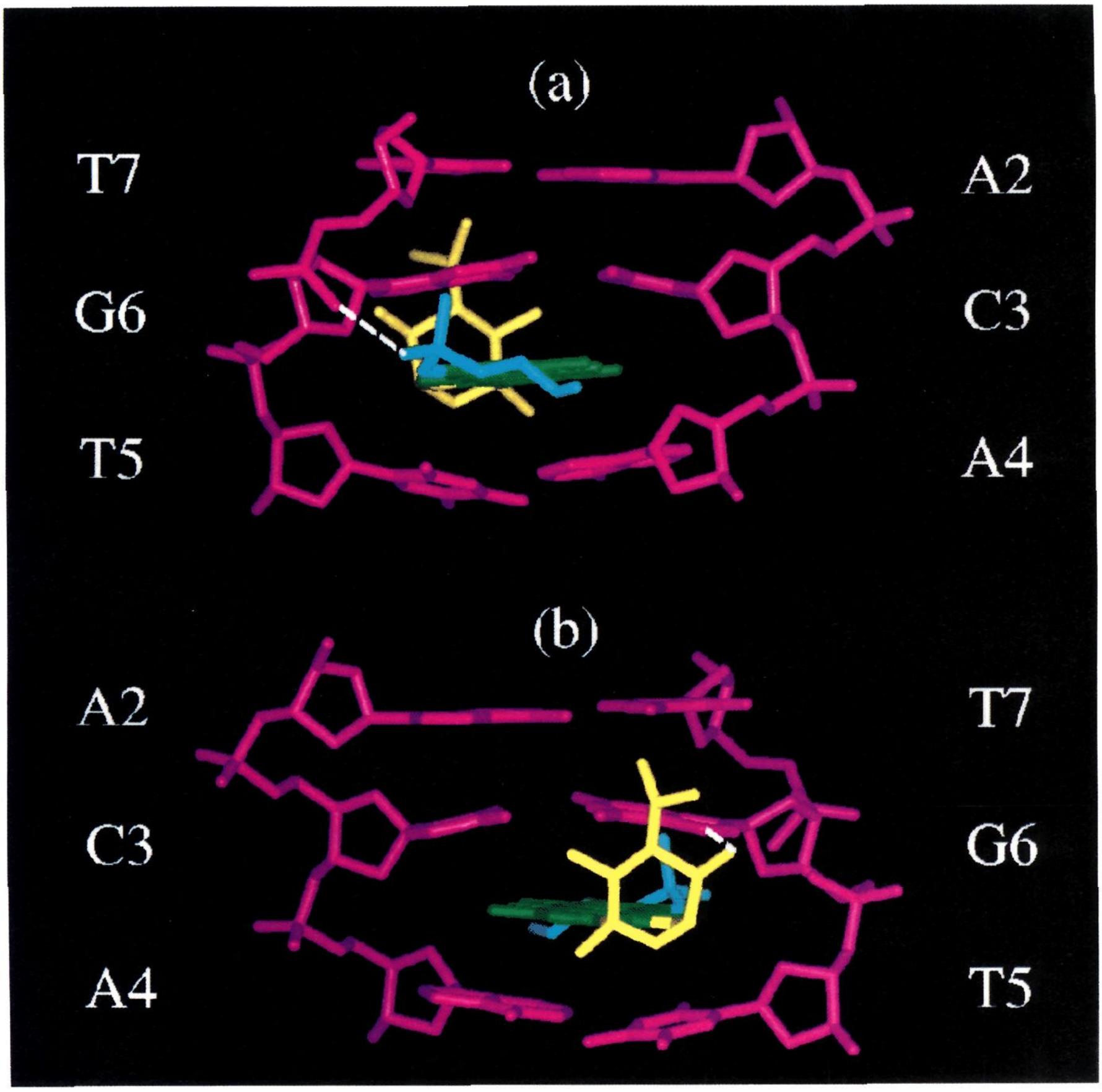

Figure 8. Intermolecular hydrogen bonds between the menogaril molecule and the DNA in the menogaril−d(G-A-C-A-T-G-T-C) complex (two drugs per duplex). The DNA is in magenta. Menogaril aromatic rings B, C, and D of the aglycon are in green, nonplanar cyclohexene ring A of the aglycon is in blue, and the bicyclic aminoglucose sugar is in yellow. (a) This hydrogen bond is found in the minor groove of the DNA and is from M(OH-9) to the oxygen atom of the G6-T7 phosphate group. The donor−acceptor distance is 1.67 Å. (b) This hydrogen bond is found in the major groove of the DNA and is between the M(OH-2″) and G6(N7). The donor−acceptor distance is 1.8 Å.

Table 6. Intermolecular Hydrogen Bond Distances and Angles in the Menogaril−d(G-A-C-A-T-G-T-C) Complex (Two Drugs per Duplex)

donor−acceptor	distance (Å)	angle (deg)
M(OH-2″)−G6(N7)	$1.84 \pm 0.04^{a,d}$	$172.6 \pm 0.8^{b,d}$
M(OH-9)−T7(O2P)	1.59 ± 0.03^{a}	177.9 ± 0.8^{c}

[a] Distance is between donor hydrogen and acceptor heteroatom. [b] Angle corresponds to atoms O−H- - -N. [c] Angle corresponds to atoms O−H- - -O. [d] We only observe this hydrogen bond for three out of the four structures. The distance and angle values were calculated for these three structures.

unwinding of 9° between symmetry-related (A2-C3)•(G6-T7) steps in the complex.

The central A4•T5 base pairs are propeller-twisted by 13° (Figure 6f) in contrast to smaller propeller twists at the remaining nonterminal A2•T7 and C3•G6 base pairs in the complex. The base pair stacking at the pur(3′−5′)pyr (A4-T5)•(A4-T5) step is shown in stereo in Figure 7c, and that at the (A2-C3)•(G6-T7) step is shown in stereo in Figure 7a, with greater stacking within individual strands in the former case presumably associated with more pronounced helical-unwinding and propeller-twisting at this central step.

Intermolecular Interactions in the Major Groove. The bicyclic aminoglucose sugar of menogaril is positioned in the major groove and interacts primarily with the T5-G6-T7 containing strand of the duplex (Figure 8). One face of the chair conformation of the aminoglucose sugar containing the OH-2″ and OH-4″ protons is directed toward the major groove with the bridgehead oxygen directed toward the A4•T5 base pair

while the charged $N(CH_3)_2$-3″ group is directed toward the A2·T7 base pair. These hydroxyl functionalities are involved in intermolecular hydrogen bond formation with acceptor atoms on the major groove edge of the C3·G6 base pair in the complex. Specifically, a strong hydrogen bond is detected between the OH-2″ donor hydroxyl on menogaril and the N7 acceptor on G6 (Table 6 and Figure 8b).

Additional intermolecular interactions in the major groove include hydrophobic contacts between the CH_3-5″ group and the CH_3 group of T5 in one direction (Figure 5) and electrostatic contacts between the charged $N(CH_3)_2$-3″ group and the O4 carbonyl of T7 in the opposite direction (Figure 8) in the complex.

Intermolecular Interactions in the Minor Groove. The cyclohexene ring A of menogaril adopts a half chair conformation with the out-of-plane C8 carbon directed toward the A4·T5 base pair while its out-of-plane C9 carbon neighbor is directed toward the C3·G6 base pair in the complex. TheC9-OH hydroxyl group in an equatorial orientation donates a hydrogen bond to the O2P phosphate oxygen at the G6-T7 step (Figure 8a). In essence, the intercalated aglycon of menogaril is anchored in place by intermolecular hydrogen bonds in both the major (Figure 8b) and minor (Figure 8a) grooves.

The cyclohexene ring A positioned in the minor groove does not overlap with the base pairs flanking the intercalation site in the complex (Figure 7b). Intermolecular hydrophobic interactions are contributed by the OCH_3-7 group which is directed toward the A4 sugar and the CH_3-9 and CH_2-10 groups which are directed toward the G6 sugar in the complex.

Comparison with Other Anthracycline–DNA Complexes. We have investigated the structure of the menogaril–DNA complex because of its clinical relevance as an antitumor agent[16,18] lacking the toxicity of nogalamycin[17] and because of its activity against multi-drug resistant human breast tumor cell lines.[19]

The menogaril–DNA complex reported in this study has many global structural features in common with the structures of nogalamycin–DNA complexes studied in the crystalline[12,13] and solution[14,15] states. Thus, both menogaril (**3**) and nogalamycin (**2**) intercalate preferentially at (C-A)·(T-G) sites and position the bicyclic aminoglucose sugar in the major groove. A common feature is the intermolecular hydrogen bond(s) between the hydroxyl groups on the bicyclic aminoglucose sugar and the major groove G·C edge adjacent to the intercalation site. These interactions must contribute significantly to the observed (C-A)·(T-G) and (C-G)·(C-G) sequence specificity of complex formation.

The nogalose sugar and acetyl functionality attached to aglycon ring A which are present in nogalamycin (**2**) but absent in menogaril (**3**) must not play a key role in the sequence specificity for targeting intercalation sites on DNA. Rather, these functionalities which are positioned in the minor groove must clamp the intercalated nogalamycin within the helix. There are differences in certain structural features of the intercalation site in the nogalamycin–DNA and menogaril–DNA complexes associated with the minor groove interactions in the former complex. Thus, the phosphorus resonances at the (C-A)·(T-G) intercalation sites are significantly shifted to low field in the nogalamycin–DNA complex but not in the menogaril–DNA complex.

Menogaril which intercalates into DNA through the major groove (unlike other natural intercalators which target the minor groove) could directly act as a transcription repressor for those transcription factors that target the major groove centered about (C-A)·(T-G) binding sites.

Coordinate Deposition. The coordinates of the menogaril–d(G-A-C-A-T-G-T-C) complex (two drugs per duplex) have been deposited with the Protein Data Bank, Brookhaven Laboratory, Upton, New York 11293 (accession number: 202D), from whom copies can be obtained.

Acknowledgment. This research was funded by NIH Grant CA-46778 to D.J.P.

Supplementary Material Available: One table of proton complexation chemical shifts and three figures of exchangeable and nonexchangeable proton spectra and a proton–phosphorus two-dimensional correlation plot for the menogaril–d(G-A-C-A-T-G-T-C) complex (two drugs per duplex) (5 pages). This material is contained in libraries on microfiche, immediately follows this article in the microfilm version of the journal, can be ordered from the ACS, and can be downloaded from the Internet; see any current masthead page for ordering information and Internet access instructions.

JA950489+